Multi-Objective Cooperative Control for a Ship-Towing System in Congested Water Traffic Environments

Du, Zhe; Negenborn, Rudy R.; Reppa, Vasso

DOI
10.1109/TITS.2022.3208328

Publication date
2022

Document Version
Final published version

Published in
IEEE Transactions on Intelligent Transportation Systems

Multi-Objective Cooperative Control for a Ship-Towing System in Congested Water Traffic Environments

Zhe Du, Rudy R. Negenborn, and Vasso Reppa, *Member, IEEE*

***Abstract*— This paper proposes a multi-objective cooperative control method for a ship-towing system in congested water traffic environments. The control objectives are to coordinate multiple autonomous tugboats for transporting a ship to: (i) follow the waypoints, (ii) adjust the heading, (iii) track the speed profile, and (iv) resolve collisions. The problem is tackled by the design of multiple control agents distributed in two control layers. Based on the strategy of model predictive control (MPC), the supervisory controller in the higher layer calculates the towing angles and forces of the ship, the tug controller in the lower layer computes the tug thruster forces and moment. The consensus between the lower and higher layer control is achieved by using the altering direction method of multipliers (ADMM) that makes the predicted tug position and heading approach to the desired tug trajectory. Simulation experiments indicate that the proposed method coordinates multiple autonomous tugboats to transport a ship smoothly and effectively and succeeds in multiple control objectives, in the meantime, the avoidance operation complies with COLREGS rules.**

***Index Terms*— Multi-objective control, distributed cooperative control, autonomous surface vessels (ASVs), multi-vessel ship-towing system.**

I. Introduction

THE trend of the world shipping industry is green, safe, and efficient, where Autonomous Surface Vessels (ASVs) play an important role to achieve these objectives [1]. In recent years, their development has been mitigated from fundamental research to civil and commercial uses [2]. Meanwhile, with the increasing complexity of applications, the research of ASVs has changed from single vessel to multi-vessel systems.

According to the way of connection, multi-vessel systems are classified into two types: cyber-connected and physical-connected systems [3]. In the first case, all vessels are clustered within a safe distance forming a certain formation shape. In the second case, there is a physical link (through cables or directly by attaching) between vessels, and a floating object is often involved. The above two multi-vessel systems always involve many control objectives, like waypoint (position) following, heading adjusting, and speed tracking. In some cases, the distance is also controlled to resolve collisions. Different from the other three objectives which are directly related to specific missions, speed control focuses on improving the motion by smoothing the trajectory. There is limited research working on this control objective, mostly focusing on the single vessel system, as shown in Table I.

For the speed control of a single vessel system, the main research goal is to regulate the surge speed to a constant value. In [8], scholars propose a backstepping-based adaptive speed controller to maintain a reference speed; in [9], an adaptive model predictive controller is proposed to regulate the speed of an ASV under the unknown model parameters of dynamics. Some research works have investigated both the speed and heading control of the ASV to regulate speed and heading to make them reach the corresponding reference values [4], [5], [6], [7].

For the cyber-connected vessel system, the research goal is formation control. The control objectives are mainly the position and heading. Authors in [10], [11], and [12] use the leader-follower strategy to make a swarm of ASVs follow the trajectory of a (virtual) leader vessel, where the desired relative position and heading with respect to the leader are the control objectives of the followers. Some scholars concern the collision avoidance during the moving process, they design a changeable formation that can make each vessel avoid obstacles [13], [14], [15].

For the physical-connected vessel system, the research focus is the floating object manipulation. Compared to the cyber-connected system, this type has less ability of maneuvering and more constraints on dynamics. The control objectives aim for the transported floating object. In the beginning, scholars work on transporting the object to the desired position (position control) [16], [17], [18]. Later on, as the floating object becomes specific, like a large ship, the heading of the object requires to be regulated. Authors in [19] and [20] use six ASVs to attach on a large ship and manipulate it to the desired position with the desired heading. Some scholars consider that a floating object is transported for tracking a reference path in an obstacle environment by one attached ASV and two towed ASV [21].

It is observed that there is a lack of research focusing on speed control of the multi-vessel systems. As a typical application, ship-towing transportation is an important but also challenging operation in the maritime. Usually, before

Manuscript received 1 December 2021; revised 4 July 2022; accepted 13 September 2022. Date of publication 28 September 2022; date of current version 5 December 2022. This work was supported in part by the China Scholarship Council under Grant 201806950080, in part by the Researchlab Autonomous Shipping (RAS) of Delft University of Technology, in part by the INTERREG North Sea Region Grant "AVATAR" funded by the European Regional Development Fund, and in part by the EFRO REACT-EU Op-Zuid Project "Fieldlab autonomous sailing technology (FAST)" under Grant 4119. The Associate Editor for this article was B. Ayalew. *(Corresponding author: Zhe Du.)*

The authors are with the Department of Maritime and Transport Technology, Delft University of Technology, 2628 CD Delft, The Netherlands (e-mail: z.du@tudelft.nl; r.r.negenborn@tudelft.nl; v.reppa@tudelft.nl).

Digital Object Identifier 10.1109/TITS.2022.3208328

TABLE I
CLASSIFICATION OF MULTI-VEHICLE SYSTEMS AND CONTROL AND AVOIDANCE METHODS

Research Article	Type of Vessel System			Type of Control Objective				Control Architecture	
	Single	Cyber connected	Physical connected	Position Control	Heading Control	Speed Control	Collision Avoidance	Centralized	Distributed
[4]	✓				✓	✓			✓
[5]	✓				✓	✓		✓	
[6]	✓				✓	✓			✓
[7]	✓				✓	✓			✓
[8]	✓					✓		✓	
[9]	✓					✓		✓	
[10]		✓		✓	✓				✓
[11]		✓		✓	✓				✓
[12]		✓		✓	✓				✓
[13]		✓		✓	✓		✓		✓
[14]		✓		✓	✓		✓		✓
[15]		✓		✓	✓		✓		✓
[16]			✓	✓					✓
[17]			✓	✓					✓
[18]			✓	✓					✓
[19]			✓	✓	✓			✓	
[20]			✓	✓	✓			✓	
[21]			✓	✓	✓		✓		✓
This paper			✓	✓	✓	✓	✓		✓

carrying out the towage, speed recommendations are given for dealing with emergencies [22], [23]. From the viewpoint of collision avoidance, all the vessels that take actions of avoidance should comply with standards of global regulations called "The International Regulations for Preventing Collisions at Sea", shortly COLREGS [24]. In the regulation, rules 13-17 are usually considered by scholars, but rule 6, which requests a safe speed for every vessel, is ignored. Thus, it is necessary to consider the speed control for a ship-towing system.

From the point of the control architecture shown in Table I, the research of the single-vessel system adopts both centralized (for only one control objective) and distributed (for two control objectives) ones. While for the multi-vessel systems, the architecture is usually the distributed control, because compared to the centralized one this architecture is better in scalable application scenarios and tolerance to failures [25].

In previous works, the authors have investigated different control objectives for a ship-towing system: the position and heading control [3], [26], the distance control (collision resolution) [27], [28], and the speed control [29]. However, no research considers how to coordinate properly for these control objectives to implement all of them effectively. Therefore, the contribution of this work is to propose a multi-objective cooperative control scheme for a physical-connected multi-vessel towing system. Moreover, a set of key performance indicators is defined to check to what extent these objectives are achieved. The proposed control scheme coordinates the multiple autonomous tugboats to make the floating object follow the waypoints, adjust the heading, track the speed profile, and resolve collisions. In the meantime, the avoidance operation complies with COLREGS rules (Rules 6 and 13-17).

The remainder of this paper is organized as follows. Section II formulates the main problem and the kinematics and kinetics model of the towing system. The design of the proposed control scheme and the definition of a set of key performance indicators are given in Section III. In Section IV, simulation experiments are carried out for representative situations to illustrate the potential of the proposed scheme. Conclusions and future research directions are given in Section V.

II. PROBLEM STATEMENT AND SYSTEM MODELING

The towing system considered in this paper consists of three vessels, two ASVs are the tugboats located at the front and rear of an unpowered ship providing power: the role of the front one is to increase the speed and adjust the heading of the ship, and the role of the other one is to decrease the speed and steady the heading of the ship. The motion of each individual vessel is represented by the 3-DOF hydrodynamic model [30]:

$$\begin{aligned}\dot{\boldsymbol{\eta}}_*(t) &= \boldsymbol{R}\big(\psi_*(t)\big)\boldsymbol{v}_*(t) \\ &\quad \times \boldsymbol{M}_*\dot{\boldsymbol{v}}_*(t) + \boldsymbol{C}_*\big(\boldsymbol{v}_*(t)\big)\boldsymbol{v}_*(t) + \boldsymbol{D}_*\big(\boldsymbol{v}_*(t)\big)\boldsymbol{v}_*(t) \\ &= \boldsymbol{\tau}_*(t), \end{aligned} \tag{1}$$

where $*$ stands for S (ship) or i (tug, $i = 1, 2$); $\boldsymbol{\eta}_*(t) = [x_*(t)\ y_*(t)\ \psi_*(t)]^{\mathrm{T}} \in \mathbb{R}^3$ is the position vector in the world frame (North-East-Down) including position coordinates $\big(x_*(t),\ y_*(t)\big)$ and heading $\psi_*(t)$; $\boldsymbol{v}_*(t) = [u_*(t)\ v_*(t)\ r_*(t)]^{\mathrm{T}} \in \mathbb{R}^3$ is the velocity vector in the body-fixed frame containing the velocity of surge $u_*(t)$, sway $v_*(t)$ and

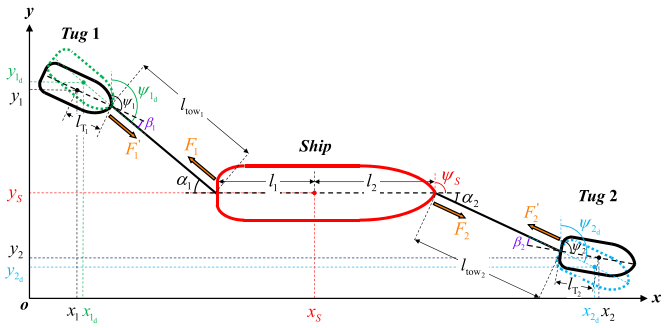

Fig. 1. Geometrical relationship between the ship and tugs.

yaw $r_*(t)$; $\boldsymbol{R} \in \mathbb{R}^{3\times3}$ is the rotation matrix from the body frame to the world frame, which is a function of heading:

$$\boldsymbol{R}\big(\psi_*(t)\big) = \begin{bmatrix} \cos\big(\psi_*(t)\big) & -\sin\big(\psi_*(t)\big) & 0 \\ \sin\big(\psi_*(t)\big) & \cos\big(\psi_*(t)\big) & 0 \\ 0 & 0 & 1 \end{bmatrix}; \quad (2)$$

$\boldsymbol{M}_* \in \mathbb{R}^{3\times3}$, $\boldsymbol{C}_* \in \mathbb{R}^{3\times3}$ and $\boldsymbol{D}_* \in \mathbb{R}^{3\times3}$ are the mass (inertia), Coriolis-Centripetal and damping matrices; $\boldsymbol{\tau}_*(t) = [\tau_{*\mathrm{u}}(t)\ \tau_{*\mathrm{v}}(t)\ \tau_{*\mathrm{r}}(t)]^{\mathrm{T}} \in \mathbb{R}^3$ is the controllable input referring to the forces $\tau_{*\mathrm{u}}(t)$, $\tau_{*\mathrm{v}}(t)$ and moment $\tau_{*\mathrm{r}}(t)$ in the body-fixed frame. This model decomposes the motion of a vessel into forwarding (surge) and steering (sway and yaw) parts. So the speed control in this paper refers to regulating the magnitude of the surge velocity.

A. Kinematics of the Towing System

Assuming the desired elongation of the towline l_{tow_i} that guarantees the action of the restoring forces and the collision avoidance between the transported ship and the two tugs, the configuration of the towing system can be determined by the geometrical relationship of the three vessels [26]. As shown in Fig. 1, the desired position and heading of tug i ($\boldsymbol{\eta}_{i_{\mathrm{d}}}(t) = [x_{i_{\mathrm{d}}}(t)\ \ y_{i_{\mathrm{d}}}(t)\ \ \psi_{i_{\mathrm{d}}}(t)]^{\mathrm{T}}$, $i = 1, 2$) are calculated by

$$\boldsymbol{\eta}_{i\mathrm{d}}(t) = \boldsymbol{\eta}_S(t) + (l_{\mathrm{tow}_i} + l_{\mathrm{T}_i})\boldsymbol{E}_i\big(\psi_S(t), \alpha_i(t)\big) + l_i\boldsymbol{H}_i\big(\psi_S(t)\big) + \alpha_i(t)[0\ \ 0\ \ 1]^{\mathrm{T}}, \quad (3)$$

where $\boldsymbol{\eta}_S(t)$ is the position and heading of the ship; l_{T_i} is the distance from the center of gravity of the tug to its bow (l_{T_1} for Tug 1) or stern (l_{T_2} for Tug 2); l_i is the distance from the center of gravity of the ship to its stern (l_1) or its bow (l_2); $\alpha_i(t)$ is the towing angle; $\boldsymbol{E}_i \in \mathbb{R}^3$ and $\boldsymbol{H}_i \in \mathbb{R}^3$ are the vectors related to the heading of the ship and the towing angles, formulated as:

$$\boldsymbol{E}_i = (-1)^i \begin{bmatrix} \sin\big(\psi_S(t) + \alpha_i(t)\big) \\ \cos\big(\psi_S(t) + \alpha_i(t)\big) \\ 0 \end{bmatrix}, \quad (4)$$

$$\boldsymbol{H}_i = (-1)^i \begin{bmatrix} \sin\big(\psi_S(t)\big) \\ \cos\big(\psi_S(t)\big) \\ 0 \end{bmatrix}. \quad (5)$$

Equations (3)-(5) show that the desired tug trajectory $\boldsymbol{\eta}_{i\mathrm{d}}(t)$ is calculated based on the ship position vector $\boldsymbol{\eta}_S(t)$ and the ship towing angles $\alpha_i(t)$.

B. Kinetics of the Towing System

According to the 3-DoF hydrodynamic model (1), the key to the kinetics of the towing system is to model the controllable inputs $\boldsymbol{\tau}_*(t)$ [3].

For the manipulated ship, the controllable inputs ($\boldsymbol{\tau}_S(t)$) are the forces and moment from the towing lines applied by the two tugs (seen in Fig. 1), which can be expressed as:

$$\boldsymbol{\tau}_S(t) = \boldsymbol{\tau}_{S_1}(t) + \boldsymbol{\tau}_{S_2}(t) = \sum_{i=1}^{2} \boldsymbol{B}_S\big(\alpha_i(t)\big)F_i(t), \quad (6)$$

where $F_i(t)$ is the towing forces; $\boldsymbol{B} \in \mathbb{R}^3$ is the configuration matrix which is a function of the towing angle:

$$\boldsymbol{B}_S = \begin{bmatrix} \cos\big(\alpha_i(t)\big) \\ \sin\big(\alpha_i(t)\big) \\ l_i\sin\big(\alpha_i(t)\big) \end{bmatrix} \quad (i = 1, 2). \quad (7)$$

For the i-th tug, the controllable inputs denoted by $\boldsymbol{\tau}_i$ are the thruster forces and moment (omnidirectional forces generated by azimuth thrusters [31]), expressed as:

$$\boldsymbol{\tau}_i(t) = \boldsymbol{B}_i\big(\beta_i(t)\big)F_i'(t) + \boldsymbol{\tau}_{T_i}(t), \quad (8)$$

where $\boldsymbol{B}_i \in \mathbb{R}^3$ is the configuration matrix of the tug i, which is a function of the tug angle $\beta_i(t)$:

$$\boldsymbol{B}_i = \begin{bmatrix} \cos\big(\beta_i(t)\big) \\ \sin\big(\beta_i(t)\big) \\ l_{\mathrm{T}_i}\sin\big(\beta_i(t)\big) \end{bmatrix} \quad (i = 1, 2); \quad (9)$$

$\beta_i(t)$ is the deviation between the actual and desired heading of the tugs, calculated by:

$$\beta_i(t) = \psi_S(t) + \alpha_i(t) - \psi_i(t); \quad (10)$$

$\boldsymbol{\tau}_{T_i}(t) \in \mathbb{R}^3$ is the forces and moment to move the tug i; $F_i'(t)$ is the force applied through a controlled winch onboard the tugboat to the towline (seen in Fig. 1). Assuming no force loss on the towline, then $F_i'(t) \equiv F_i(t)$. In this work, we do not consider the bottom-level winch control and the detailed model of the force F_i as a function of the elastic elongation and the generalized stiffness that depends on the material, diameter and the strand construction of the towline [32].

III. Multi-Objective Control Scheme

The basic idea of the multi-objective cooperative control scheme is to design controllers with different objectives distributed in two control layers.

As shown in Fig. 2, in the higher-layer, according to the desired position, heading $\boldsymbol{\eta}_{S\mathrm{d}}(t)$ and speed $\boldsymbol{\nu}_{S\mathrm{d}}(t)$ of the ship output from the ship reference system, the obstacle information $\boldsymbol{\eta}_{ob}(t)$, and the current states of the ship $\boldsymbol{\eta}_S(t)$, $\boldsymbol{\nu}_S(t)$, the supervisory controller (located on the ship) carries out the tasks of waypoints following, speed profile tracking, and collision resolution for the transported ship. Meanwhile, it outputs the predicted ship surge speed $u_{S_{\mathrm{P}}}(t)$, the predicted towing forces $F_{i_{\mathrm{P}}}(t)$, and the desired tug trajectory $\boldsymbol{\eta}_{i\mathrm{d}}(t)$ (which is a function of the predicted towing angles $\alpha_{i_{\mathrm{P}}}(t)$). The tug controller (located on the tugs) uses this data, the obstacle information, and the current states of tugs $\boldsymbol{\eta}_i(t)$, $\boldsymbol{\nu}_i(t)$

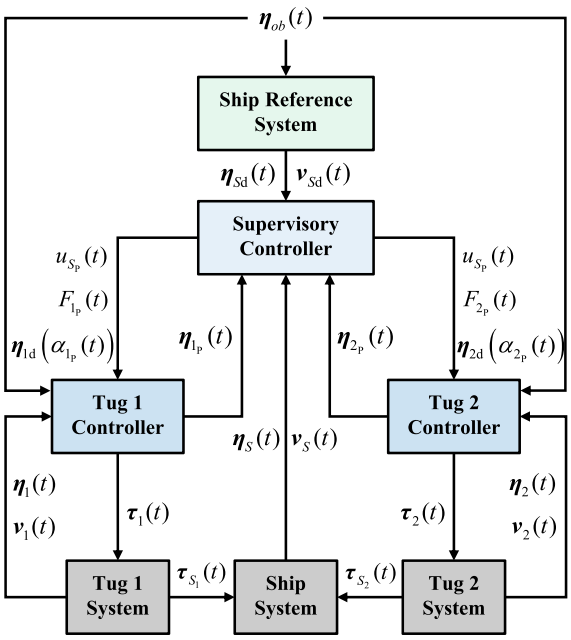

Fig. 2. System control diagram.

to perform the tasks of trajectory and surge speed tracking, and collision resolution. In order to reach a consensus between the lower-layer and higher-layer control, the tug controller first outputs the predicted tug position and heading $\eta_{i\mathrm{P}}(t)$ and shares them with the supervisory controller. Then, both higher and lower layer controllers update the corresponding data to make the predicted tug position and heading approach to the desired tug trajectory as much as possible ($\eta_{i\mathrm{P}}(t) \to \eta_{i\mathrm{d}}(t)$). When the consensus is achieved, the tug controller outputs the thruster forces and moment $\boldsymbol{\tau}_i(t)$ to the tug system. Based on the calculated thruster propulsion, the two autonomous tugs cooperatively provide manipulating forces and moment ($\boldsymbol{\tau}_{S_1}(t)$, $\boldsymbol{\tau}_{S_2}(t)$) to make the ship achieve multiple objectives.

A. Ship Reference System

The ship reference system is to provide the reference position, heading, and surge speed of the manipulated ship, which are determined by comparing between the detection distance d_{D} and obstacle distance $d_{\mathrm{ob}}(t)$, expressed as:

$$\begin{cases} \boldsymbol{\eta}_{S\mathrm{d}}(t) = \boldsymbol{\eta}_{Sq}, \quad \boldsymbol{v}_{S\mathrm{d}}(t) = \boldsymbol{v}_{Sq} \quad d_{\mathrm{ob}}(t) > d_{\mathrm{D}} \\ \boldsymbol{\eta}_{S\mathrm{d}}(t) = \boldsymbol{\eta}_{S\mathrm{n}}, \quad \boldsymbol{v}_{S\mathrm{d}}(t) = \boldsymbol{v}_{S\mathrm{n}} \quad d_{\mathrm{ob}}(t) \le d_{\mathrm{D}} \end{cases}$$
$$d_{\mathrm{ob}}(t) = \min\left\{d_{Sj}(t), d_{1j}(t), d_{2j}(t)\right\}, \tag{11}$$

where $\boldsymbol{\eta}_{Sq}$ and $\boldsymbol{v}_{Sq}$ are the predefined position and velocity references of waypoint q; $\boldsymbol{\eta}_{S\mathrm{n}}$ and $\boldsymbol{v}_{S\mathrm{n}}$ are the new (updated) position and velocity references; $d_{Sj}(t)$, $d_{1j}(t)$, and $d_{2j}(t)$ are the distances from the obstacle j to the manipulated ship, to the tug 1, and to the tug 2, respectively. Such a definition of the obstacle distance $d_{\mathrm{ob}}(t)$ in (11) is the reason that the three vessels in the towing system are indivisible systems, the risk from the obstacles should be alert by the closest vessel.

The new reference $\boldsymbol{\eta}_{Sn}$ is calculated based on the COLREGS Rules 13-17, where Rules 13 to 15 provide definitions and operations of the situations of overtaking, head-on, and crossing that a single vessel may encounter; Rule 16 describes the generic actions that the give-way vessels should take; Rule 17 indicates the actions that the stand-on vessels should take. While for the multiple vessels in the towing system, the above operations can be equivalently converted to taking advantage of the waypoint clockwise altering to calculate the new position and heading, expressed as:

$$\boldsymbol{\eta}_{S\mathrm{n}} = \begin{bmatrix} x_{S\mathrm{n}} \\ y_{S\mathrm{n}} \\ \psi_{S\mathrm{n}} \end{bmatrix} = \begin{bmatrix} x_{Sq-1} \\ y_{Sq-1} \\ \psi_{Sq} \end{bmatrix} + r \begin{bmatrix} \sin(\theta) \\ \sin(\theta) \\ \theta/r \end{bmatrix}$$
$$r = \left\| \begin{bmatrix} x_{Sq-1} \\ y_{Sq-1} \end{bmatrix} - \begin{bmatrix} x_{Sq} \\ y_{Sq} \end{bmatrix} \right\|_2, \tag{12}$$

where x_{Sq-1} and y_{Sq-1} are the coordinates of the last waypoint $q-1$; x_{Sq} and y_{Sq} are the coordinates of the current waypoint q; r is the distance between the above two waypoints; ψ_{Sq} is the current predefined heading along the waterway direction; θ is the altering angle satisfying $0^\circ < \theta < \theta_{\max}$, where the lower boundary is for clockwise rotation, and the upper boundary is defined based on spatial constraint ($\theta_{\max} = \arctan(d(t)/l(t))$, where $l(t)$ is the distance between two waypoints; $d(t)$ is the minimum distance from the predefined path to the edge of the spatial boundaries).

The new reference $\boldsymbol{v}_{S\mathrm{n}}$ is updated according to the COLREGS Rule 6. This rule suggests a safe speed for every vessel to make sure it can take proper and effective action to avoid collisions. Although Rule 8 points out that altering only the course may be the most effective action to avoid a close-quarters situation with sufficient sea room, this is in the case of a single vessel. For a physical-connected multi-vessel system, a safe speed can guarantee more response time for such a motion-restricted system taking actions of avoidance. Thus, the updated speed profile is defined as:

$$\boldsymbol{v}_{S\mathrm{n}} = \begin{bmatrix} u_{S\mathrm{n}} \\ v_{S\mathrm{n}} \\ r_{S\mathrm{n}} \end{bmatrix} = \begin{bmatrix} a_u & & \\ & 1 & \\ & & 1 \end{bmatrix} \begin{bmatrix} u_{Sq} \\ v_{Sq} \\ r_{Sq} \end{bmatrix}, \tag{13}$$

where u_{Sq}, v_{Sq} and r_{Sq} are the current surge, sway and yaw speed profiles, respectively; a_u is the speed reduction coefficient and $0 < a_u < 1$. From (13), the speed profile update is to slow down the surge speed. The value of a_u is determined by the relative position, course, and velocity between the ship and obstacles, which belongs to the research of the risk assessment and is out of the scope in this paper.

B. Supervisory Controller

The control objectives of the supervisory controller are to make the ship follow waypoints, track speed profile, and resolve collision; the control inputs include two towing angles and two towing forces; while the constraints include the ship dynamics, the actuator saturation, and the system configuration. For the collision resolution task, it is required to take actions in advance for such a low maneuverability system. Thus, this is a problem of multiple objectives, multiple inputs, and multiple constraints with required predictive action. Based on the above analysis, the model predictive control (MPC) is applied as the control strategy.

The core of the MPC-based controller is to design the optimizer, which solves the following optimization problem to get control inputs of the ship U_S:

$$\min_{\boldsymbol{\tau}_S} \sum_{h=1}^{H_\mathrm{P}} J_S(k+h|k), \tag{14}$$

subject to *i)* Ship dynamics, *ii)* Actuator saturation, *iii)* Configuration restriction,

where H_P is the length of the prediction horizon; k is the current time instant; h is the hth time prediction step; $J_S(k+h|k)$ are the prediction made at k about the cost function of the ship at $k+h$. Before discussing the optimizer constraints i) to iii), the performance function J_S is first designed as:

$$\begin{aligned} J_S(k) &= \boldsymbol{e}_{\eta S}^{\mathrm{T}}(k)\boldsymbol{W}_{S1}\boldsymbol{P}_S(k)\boldsymbol{e}_{\eta S}(k) \\ &\quad + \boldsymbol{e}_{\nu_S}^{\mathrm{T}}(k)\boldsymbol{W}_{S2}\boldsymbol{e}_{\nu_S}(k) \\ &\quad + W_{S3}\sum_{j=1}^{n}\left(d_{Sj}(k) - d_{S\mathrm{safe}}\right)^{-2} \\ \boldsymbol{e}_{\eta S}(k) &= \boldsymbol{\eta}_{S_\mathrm{P}}(k) - \boldsymbol{\eta}_{S_\mathrm{d}}(k) \\ \boldsymbol{e}_{\nu_S}(k) &= \boldsymbol{\nu}_{S_\mathrm{P}}(k) - \boldsymbol{\nu}_{S_\mathrm{d}}(k), \end{aligned} \tag{15}$$

where $\boldsymbol{\eta}_{S_\mathrm{P}}(k) \in \mathbb{R}^3$ and $\boldsymbol{\nu}_{S_\mathrm{P}}(k) \in \mathbb{R}^3$ are the predicted position and velocity of the ship; n is the number of obstacles; d_{S_safe} is the safe distance between the ship and obstacles ($d_{S_\mathrm{safe}} < d_\mathrm{D}$), the details of the calculation can be found in [27]. The terms $\boldsymbol{W}_{S1}$, $\boldsymbol{W}_{S2}$ and W_{S3} are the weight coefficients: $\boldsymbol{W}_{S1} = \mathrm{diag}(w_{Sx}\ w_{Sy}\ w_{S\psi})$ and $\boldsymbol{W}_{S2} = \mathrm{diag}(w_{Su}\ w_{Sv}\ w_{Sr})$ are the positive diagonal matrices, W_{S3} is the positive scalar; $\boldsymbol{P}_S(k)$ is the ship weight factor. The performance function (15) contains three parts: the position error is minimized to achieve waypoints following, the velocity error is minimized to track the speed profile, the reciprocal distance error is minimized to keep away from the obstacles.

At the beginning of the waypoint following process, the value of the position error between the manipulated ship and the waypoint is maximum. In order to make the manipulated ship approach the waypoint for reducing the position error, the supervisory controller forces the front tugboat to increase the towing force to increase the speed of the platform. As the ship gradually approaches the waypoint, the position error is getting smaller, and the speed of the platform is reduced accordingly. The supervisory controller, on the other hand, has to regulate the speed of the manipulated ship to track the speed profile. Thus, minimizing the position error and velocity error simultaneously is the main conflict of the used multiple objectives in this work. Thus, the ship weight factor $\boldsymbol{P}_S(k)$ is designed to normalize the order of magnitude between the position and velocity errors, and to reduce the sensitivity of the controller to the waypoint distance, expressed as:

$$\begin{aligned} \boldsymbol{P}_S(t) &= \begin{bmatrix} 1/\left(d_{S_p}(t)+d_0\right) & & \\ & 1/\left(d_{S_p}(t)+d_0\right) & \\ & & 1 \end{bmatrix} \\ d_{S_p}(t) &= \sqrt{\left(x_S(t)-x_{S\mathrm{d}_p}\right)^2 + \left(y_S(t)-y_{S\mathrm{d}_p}\right)^2}, \end{aligned} \tag{16}$$

where $d_{S_p}(t)$ is the distance from current position of the ship $\left(x_S(t), y_S(t)\right)$ to the current waypoint W_p coordinates $(x_{S\mathrm{d}_p}, y_{S\mathrm{d}_p})$; d_0 is a small positive real number, which is to prevent the denominator in (16) is zero when the current position of the ship is exactly located on the current waypoint ($d_{S_p}(t) = 0$).

The ship dynamics (the first constraint) is represented by the prediction model, which determines the predicted position and velocity of the ship. They are calculated by discretizing the dynamic model (1) with a sample time T_s:

$$\begin{aligned} \boldsymbol{\eta}_{S_\mathrm{P}}(k+1) &= \boldsymbol{\eta}_{S_\mathrm{P}}(k) + \int_{kT_s}^{(k+1)T_s} \boldsymbol{R}\left(\psi_S(t)\right)\boldsymbol{\nu}_S(t)dt \\ \boldsymbol{\nu}_{S_\mathrm{P}}(k+1) &= \boldsymbol{\nu}_{S_\mathrm{P}}(k) + \int_{kT_s}^{(k+1)T_s} \boldsymbol{M}_S^{-1}\Big[-\boldsymbol{C}_S\left(\boldsymbol{\nu}_S(t)\right)\cdot \\ &\quad \times \boldsymbol{\nu}_S(t) - \boldsymbol{D}_S\left(\boldsymbol{\nu}_S(t)\right)\boldsymbol{\nu}_S(t) \\ &\quad + \sum_{i=1}^{2} \boldsymbol{B}_S\left(\alpha_i(t)\right)F_i(t)\Big]dt. \end{aligned} \tag{17}$$

The actuator saturation (the second constraint) stem from the physical laws and maritime practice [31]. For all k over the prediction horizon:

$$-\alpha_{i\,\max} \le \alpha_i(k) < \alpha_{i\,\max} \tag{18}$$

$$0 \le F_i(k) \le F_{i\,\max} \tag{19}$$

$$|\dot{\alpha}_i(k)| \le \bar{\alpha}_i \tag{20}$$

$$\left|\dot{F}_i(k)\right| \le \bar{F}_i, \tag{21}$$

where $\alpha_{i\,\max}$ is the maximum value of towing angle; $F_{i\,\max}$ is the maximum value of towing force that the two towing lines withstand; $\bar{\alpha}_i$ and $\bar{F}_i$ are the maximum change rate value of towing angle and force, respectively.

The configuration restriction (the third constraint) is to provide desired trajectories for tugs and reach the consensus between the higher and lower-level control to achieve the distributed control architecture. The desired position and heading of tugs are calculated by (3), the process of reaching the consensus is illustrated in subsection III-D.

Remark (Multi-Objective Optimization in MPC): The ways to solve multi-objective optimization problems can be classified into two categories: Scalarization-based methods and Pareto-based methods [33]. The first methods usually consider an overarching objective function to express all the objective components. These methods are computationally efficient but they do not always find solutions because of the objective conflicts. The Pareto-based methods search the optimal solutions space first and then choose an optimal solution from the Pareto optimal set. They can cope with the objective conflicts, but the search process requires a high computation burden.

For the multi-objective cooperative control problems in the framework of MPC, the Scalarization-based methods are usually applied. To ensure the existence of the solutions, the weights and constraints in the cost function are adjusted. Research works in [34] propose a dynamic weight adjusting strategy for the control objectives of trajectory tracking and driver's commands matching to address the conflict between the driver and the automation. In [35], scholars replace the

hard constraints with soft constraints for the battery state of charge for the aircraft microgrids to improve the feasibility of the solution of the mixed-integer linear programming (MILP)-based MPC algorithm. Authors in [36] propose a dynamic weight tuning strategy according to the inter-vehicular states to optimize the responsiveness of collision avoidance during the transitional maneuver for improving the feasibility.

In this work, in order to realize the online calculation of control inputs, the Scalarization-based method is used to speed up the computation process. However, as mentioned above, Scalarization methods create objective conflicts. In our case, this conflict happens between the position and velocity errors. For that, we design the weight factor $\boldsymbol{P}_S(k)$ *to solve it.*

C. Tug Controller

The control objectives of the tug controller are to make the tugs track their trajectories, track the predicted ship surge speed, and resolve collisions; the control inputs are thruster forces and moment containing three elements; while the constraints include the tug dynamics, the actuator saturation, and the system configuration. Thus, the control strategy also adopts the MPC.

The optimization of solving control inputs of the tug i is expressed as:

$$\min_{\boldsymbol{\tau}_{T_i}} \sum_{h=1}^{H_\mathrm{P}} J_i(k+h|\,k), \tag{22}$$

subject to *i)* Ship dynamics, *ii)* Actuator saturation, *iii)* Configuration restriction,
where the performance function J_i is designed as:

$$\begin{aligned} J_i(k) &= \boldsymbol{e}_{\eta_i}^{\mathrm{T}}(k)\boldsymbol{W}_{i1}\boldsymbol{e}_{\eta_i}(k) + \boldsymbol{e}_{\nu_i}^{\mathrm{T}}(k)\boldsymbol{W}_{i2}\boldsymbol{e}_{\nu_i}(k) \\ &\quad + W_{i3}\sum_{j=1}^{n}\left(d_{ij}(k) - d_{i\mathrm{safe}}\right)^{-2} \\ \boldsymbol{e}_{\eta_i}(k) &= \boldsymbol{\eta}_{i\mathrm{p}}(k) - \boldsymbol{\eta}_{i\mathrm{d}}(k) \\ \boldsymbol{e}_{\nu_i}(k) &= \boldsymbol{\nu}_{i\mathrm{p}}(k) - \boldsymbol{\nu}_{i\mathrm{d}}(k), \end{aligned} \tag{23}$$

where $\boldsymbol{\eta}_{S_\mathrm{p}}(k) \in \mathbb{R}^3$ and $\boldsymbol{\nu}_{i\mathrm{p}}(k) \in \mathbb{R}^3$ are the predicted position and velocity of the tug i; $\boldsymbol{\nu}_{i\mathrm{d}}(k) = [u_{S\mathrm{p}}(t)\ \ 0\ \ 0]^{\mathrm{T}} \in \mathbb{R}^3$ is the desired velocity of the tug i; n is the number of obstacles; $d_{i\mathrm{safe}}$ is the safe distance between the tug i and obstacles; $\boldsymbol{W}_{i1}$, $\boldsymbol{W}_{i2}$ and W_{i3} are the weight coefficients: $\boldsymbol{W}_{i1} = \mathrm{diag}(w_{ix}\ w_{iy}\ w_{i\psi})$ and $\boldsymbol{W}_{i2} = \mathrm{diag}(w_{iu}\ w_{iv}\ w_{ir})$ are the positive diagonal matrices, W_{i3} is the positive scalar.

The dynamics constraint is calculated by discretizing the predicted tug dynamic model with a sample time T_s:

$$\begin{aligned} \boldsymbol{\eta}_{i\mathrm{p}}(k+1) &= \boldsymbol{\eta}_{i\mathrm{p}}(k) + \int_{kT_s}^{(k+1)T_s} \boldsymbol{R}\big(\psi_i(t)\big)\boldsymbol{\nu}_i(t)dt \\ \boldsymbol{\nu}_{i\mathrm{p}}(k+1) &= \boldsymbol{\nu}_{i\mathrm{p}}(k) + \int_{kT_s}^{(k+1)T_s} \boldsymbol{M}_i^{-1}\Big[-\boldsymbol{C}_i\big(\boldsymbol{\nu}_i(t)\big)\cdot \\ &\quad \times \boldsymbol{\nu}_i(t) - \boldsymbol{D}_i\big(\boldsymbol{\nu}_i(t)\big)\boldsymbol{\nu}_i(t) + \boldsymbol{B}_i\big(\beta_i(t)\big)F_i'(t) \\ &\quad + \boldsymbol{\tau}_{T_i}(t)\Big]dt. \end{aligned} \tag{24}$$

The tug actuator saturation for all k over the prediction horizon and $i = 1, 2$:

$$-\boldsymbol{\tau}_{i\max} \le \boldsymbol{\tau}_i(k) \le \boldsymbol{\tau}_{i\max} \tag{25}$$

$\boldsymbol{\tau}_{i\max}$ is the maximum value of the thruster forces and moment.

The configuration restriction is used to achieve the distributed control architecture, illustrated in the next subsection.

D. Distributed Control Architecture

The distributed control architecture is achieved by using the Altering Direction Method of Multipliers (ADMM). This is an approach of dividing a global optimization problem into several small local optimization problems and reaching a consensus among multiple agents [37]. For our case, three optimization problems need to be solved in different controllers, and the configuration restriction requires to be considered for each controller to reach a global consensus. Thus, based on the ADMM, the iteration procedure at time instant k can be formulated as follows:

$$\begin{aligned} \boldsymbol{\tau}_{T_i}^s(k) :&= \arg\min_{\boldsymbol{\tau}_{T_i}(k)} \Bigg(J_i\big(\boldsymbol{\tau}_{T_i}(k)\big) + \lambda_i^{s-1}(k)^{\mathrm{T}}\Big[g_i\big(\boldsymbol{\tau}_{T_i}(k)\big) \\ &\quad - f_i\big(\boldsymbol{\tau}_S^{s-1}(k)\big)\Big] + (\rho_i/2)\Big\|g_i\big(\boldsymbol{\tau}_{T_i}(k)\big) \\ &\quad - f_i\big(\boldsymbol{\tau}_S^{s-1}(k)\big)\Big\|_2^2\Bigg), \end{aligned} \tag{26}$$

$$\begin{aligned} \boldsymbol{\tau}_S^s(k) :&= \arg\min_{\boldsymbol{\tau}_S(k)} \Bigg(J_S\big(\boldsymbol{\tau}_S(k)\big) + \sum_{i=1}^{2}\Big(-\lambda_i^{s-1}(k)^{\mathrm{T}} f_i\big(\boldsymbol{\tau}_S(k)\big) \\ &\quad + (\rho_i/2)\Big\|g_i\big(\boldsymbol{\tau}_{T_i}^s(k)\big) - f_i\big(\boldsymbol{\tau}_S(k)\big)\Big\|_2^2\Big)\Bigg), \end{aligned} \tag{27}$$

$$\lambda_i^s(k) := \lambda_i^{s-1}(k) + \rho_i\Big(g_i\big(\boldsymbol{\tau}_{T_i}^s(k)\big) - f_i\big(\boldsymbol{\tau}_S^s(k)\big)\Big), \tag{28}$$

where $\lambda_i(k)$ is the lagrange multiplier (dual variable); ρ_i is the penalty parameter; s is the iteration, $\cdot^s$ stands for the corresponding variable at the sth iteration; $f_i\big(\boldsymbol{\tau}_S(k)\big)$ stands for the calculation function of $\boldsymbol{\eta}_{i\mathrm{d}}(k)$, and $g_i\big(\boldsymbol{\tau}_{T_i}(k)\big)$ stands for the calculation function of $\boldsymbol{\eta}_{i\mathrm{p}}(k)$.

The termination criterion is provided based on the following residuals:

$$\begin{aligned} \Big\|\boldsymbol{R}_{\mathrm{pri},i}^s(k)\Big\|_2 &= \Big\|g_i\big(\boldsymbol{\tau}_{T_i}^s(k)\big) - f_i\big(\boldsymbol{\tau}_S^s(k)\big)\Big\|_2 \le \varepsilon_{\mathrm{pri},i}^s(k), \\ \big\|\boldsymbol{R}_{\mathrm{dual},i}^s(k)\big\|_2 &= \Big\|f_i\big(\boldsymbol{\tau}_S^s(k)\big) - f_i\big(\boldsymbol{\tau}_S^{s-1}(k)\big)\Big\|_2 \le \varepsilon_{\mathrm{dual},i}^s(k), \end{aligned} \tag{29}$$

where $\boldsymbol{R}_{\mathrm{pri},i}^s$ and $\boldsymbol{R}_{\mathrm{dual},i}^s$ are the primal and dual residual at iteration s; $\varepsilon_{\mathrm{pri},i}^s > 0$ and $\varepsilon_{\mathrm{dual},i}^s > 0$ are the feasibility tolerances, determined by

$$\begin{aligned} \varepsilon_{\mathrm{pri},i}^s(k) &= \sqrt{n_s}\varepsilon^{\mathrm{abs}} \\ &\quad + \varepsilon^{\mathrm{rel}}\max\left\{\big\|g_i\big(\boldsymbol{\tau}_{T_i}^s(k)\big)\big\|_2,\ \big\|f_i\big(\boldsymbol{\tau}_S^s(k)\big)\big\|_2\right\}, \\ \varepsilon_{\mathrm{dual},i}^s(k) &= \sqrt{n_s}\varepsilon^{\mathrm{abs}} + \varepsilon^{\mathrm{rel}}\big\|\lambda_i^s(k)\big\|_2, \end{aligned} \tag{30}$$

where n_s is the size of the variable $\boldsymbol{\tau}_{T_i}$; $\varepsilon^{\mathrm{abs}} > 0$ and $\varepsilon^{\mathrm{rel}} > 0$ are the absolute and relative tolerance, respectively.

The penalty parameter ρ_i is usually designed to be variable according to the comparison of the primal and dual residuals to increase the speed of convergence:

$$\rho_i^s = \begin{cases} \min\{2\rho_i^{s-1}, \rho_{i\max}\} & \text{if } \left\| R^s_{\text{pri},i}(k) \right\|_2 > 10 \left\| R^s_{\text{dual},i}(k) \right\|_2 \\ \max\{\rho_i^{s-1}/2, \rho_{i\min}\} & \text{if } \left\| R^s_{\text{pri},i}(k) \right\|_2 < 10 \left\| R^s_{\text{dual},i}(k) \right\|_2 \\ \rho_i^{s-1} & \text{otherwise} \end{cases} \tag{31}$$

where $\rho_{i\max}$ and $\rho_{i\min}$ are the maximum and minimum values of the penalty parameter.

Therefore, the distributed cooperative control scheme for a ship towing system is summarized in the Algorithm chart.

Algorithm -Distributed Cooperative Control Scheme

Input: Obstacle position $\boldsymbol{\eta}_{\text{ob}}(k)$; Current ship position and velocity $\boldsymbol{\eta}_S(k)$, $\boldsymbol{\nu}_S(k)$; Current tug position and velocity $\boldsymbol{\eta}_i(k)$, $\boldsymbol{\nu}_i(k)$.

Step 1: Compute a collision free path and safe speed using (11) - (13).

For $s = 1 : S$ (S is the maximum number of iterations)

Step 2: Calculate the thruster forces and moment of the tug $\boldsymbol{\tau}^s_{T_i}(k)$ in each tug local controller according to (22) - (26). Then send the results to the supervisory controller.

Step 3: Calculate the manipulation forces and moment for the ship $\boldsymbol{\tau}^s_S(k)$ in the supervisory controller according to (14) - (21) and (27).

Step 4: Update the Lagrange multiplier $\lambda^s_i(k)$ based on the results from **Step 2** and **Step 3** according to (28).

Step 5: Update the primal $\varepsilon^s_{\text{pri},i}(k)$ and dual $\varepsilon^s_{\text{dual},i}(k)$ tolerances according to (30), then check the primal $\boldsymbol{R}^s_{\text{pri},i}(k)$ and dual $\boldsymbol{R}^s_{\text{dual},i}(k)$ residuals to see whether they meet the termination criteria according to (29);

Step 6: If (29) is not satisfied, then updated the penalty parameter ρ^s_i and back to **Step 2**; otherwise, jump out of the iteration.

End

Output: Thruster forces and moment of the tug $\boldsymbol{\tau}^s_{T_i}(k)$; Manipulation forces and moment for the ship $\boldsymbol{\tau}^s_S(k)$.

E. Key Performance Indicators

Since there are multiple objectives for the designed controllers, it is necessary to define the following key performance indicators (KPIs) for checking to what extent these goals are achieved.

- Ship Waypoints Following.
  This performance is reflected by the minimum error percentage of distance from the position of the ship to each waypoint q ($q \in \{1, 2, \ldots N\}$, N is the number of waypoints), expressed as:

$$e_{P_q} = \frac{\min\left\{\sqrt{\left(x_S(k) - x_{S\text{d}_q}\right)^2 + \left(y_S(k) - y_{S\text{d}_q}\right)^2}\right\}}{\sqrt{\left(x_{S\text{d}_{q-1}} - x_{S\text{d}_q}\right)^2 + \left(y_{S\text{d}_{q-1}} - y_{S\text{d}_q}\right)^2}}, \tag{32}$$

  where $(x_{S\text{d}_{q-1}}, y_{S\text{d}_{q-1}})$ is the last waypoint coordinates and $(x_{S\text{d}_0}, y_{S\text{d}_0})$ stands for the origin coordinates (when $q = 1$). The smaller e_{P_q} indicates better following performance between waypoint $q-1$ and q.
- Ship Heading Adjusting
  At each waypoint, there is the desired heading to guide the ship sailing along the waterway. When encountering obstacles, the tugboats should manipulate the ship taking avoidance operations for safety while the desired heading becomes unimportant. Thus, different from the first indicator, what we are concerned about is the heading of the ship at the destination, so the KPI is expressed as:

$$e_\psi = \left|\psi_S(k_N) - \psi_{S\text{d}_N}\right|, \tag{33}$$

  where $\psi_{S\text{d}_N}$ is the desired ship heading at the destination; k_N is the settling time satisfying:

$$d_{S_D} < 0.25L_S; \quad \psi_S < 1^\circ; \quad u_S < 0.01 \text{ m/s}; \quad v_S < 0.01 \text{ m/s}; \quad r_S < 0.001 \text{ rad/s}.$$

  where d_{S_D} is the distance between the ship and the destination; L_S is the length of the ship.
  The smaller value of the e_ψ shows the better performance of the heading adjusting.
- Ship Speed Profile Tracking
  As the speed profile is time-varying, this KPI is calculated by the root-mean-square error (RMSE), which is expressed as:

$$e_u = \sqrt{\frac{\sum_{k=1}^{k_N}\left(u_S(k) - u_{S\text{d}}(k)\right)^2}{k_N}}, \tag{34}$$

  where the smaller value of the e_u illustrates better performance of speed profile tracking.
- Consensus reaching
  The performance of the consensus reaching can be indicated by the maximum error percentage of the towline elongation. If the elongation keeps its desired value, the consensus between the higher layer and lower layer control is well achieved. So the KPI is expressed as:

$$e_{l_i} = \left|\frac{\max\left\{l_{t_i}(k)\right\} - l_{\text{tow}_\text{i}}}{l_{\text{tow}_\text{i}}}\right|, \tag{35}$$

  where $l_{t_i}(k)$ is the distance from the towing point of the tug i to the towing point of the ship. The smaller the e_{l_i} is, the better this performance of consensus reaching is.
- Ship and Tugs Collision Resolution
  The performance of the collision resolution is reflected by the minimum distance between the three vessels and the obstacles, expressed as:

$$D_* = \min\left\{d_*(t)\right\}/L_*, \tag{36}$$

TABLE II
PARAMETERS OF THE CONTROL SYSTEM

Altering angle	$\theta = 10^\circ$
Speed reduction coefficient	$a_u = 2/3$
Prediction horizon	$H_P = 3$
Weight coefficients of J_S	$\boldsymbol{W}_{S1} = diag(1\ \ 1\ \ 1)$ $\boldsymbol{W}_{S2} = diag(200\ \ 20\ \ 20)$ $W_{S3} = 1$
Weight coefficient of J_i	$\boldsymbol{W}_{i1} = diag(1\ \ 1\ \ 1)$ $\boldsymbol{W}_{i2} = diag(2\ \ 2\ \ 2)$ $W_{i3} = 0.1$
Maximum towing angles	$\alpha_{i\max} = 45^\circ$
Maximum towing forces	$F_{i\max} = 3\text{N}$
Maximum change rate of towing angle	$\bar{\alpha}_i = 5^\circ/\text{s}$
Maximum change rate of towing forces	$\bar{F}_1 = 0.3\text{N/s}$
Maximum value of tug thruster forces	$\boldsymbol{\tau}_{i\max} = [5\text{N}\ 5\text{N}\ 2.5\text{Nm}]^{\text{T}}$
Absolute tolerance in ADMM	$\varepsilon^{\text{abs}} = 0.001$
Relative tolerance in ADMM	$\varepsilon^{\text{rel}} = 0.001$
Minimum penalty parameter in ADMM	$\rho_{i\min} = 1$
Maximum penalty parameter in ADMM	$\rho_{i\max} = 100$

TABLE III
SIMULATION SETTINGS

Initial states of the ship	W_{pO}: $\boldsymbol{\eta}_{S0} = [-15\ \ -30\ \ 0]^{\text{T}}$ $\boldsymbol{\nu}_{S0} = [0\ \ 0\ \ 0]^{\text{T}}$
Final States of the ship	W_{pD}: $\boldsymbol{\eta}_{St} = [25\ \ 30\ \ 0]^{\text{T}}$ $\boldsymbol{\nu}_{St} = [0\ \ 0\ \ 0]^{\text{T}}$
Waypoints	W_{p1}: $\boldsymbol{\eta}_{\text{p1}} = [-15\ \ -15\ \ 0]^{\text{T}}$ W_{p2}: $\boldsymbol{\eta}_{\text{p2}} = [0\ \ 0\ \ 80]^{\text{T}}$ W_{p3}: $\boldsymbol{\eta}_{\text{p3}} = [20\ \ 4\ \ 80]^{\text{T}}$ W_{p4}: $\boldsymbol{\eta}_{\text{p4}} = [25\ \ 17\ \ 0]^{\text{T}}$
Speed profile	$\text{W}_{\text{pO}} \rightarrow \text{W}_{\text{p2}}$: $\boldsymbol{\nu}_{\text{d1}} = [0.15\ \ 0\ \ 0]^{\text{T}}$ $\text{W}_{\text{p2}} \rightarrow \text{W}_{\text{pD}}$: $\boldsymbol{\nu}_{\text{d2}} = [0.09\ \ 0\ \ 0]^{\text{T}}$
Static Obstacle	Shape: Circle Radius: 1.5m Position: $(0, -4)$
Dynamic Obstacle	Shape: Ellipse Semi-major axes: 0.6m semi-minor axes: 0.15m Initial position: $(57, 20)$ Course: 260° Speed: 0.1m/s

where L_* is the length of the vessel. This KPI normalizes the distance by eliminating the effect of the vessel length. The larger of D_* shows the better performance.

These KPIs will be used in the next section to see the performance of the proposed control scheme.

IV. SIMULATION EXPERIMENTS AND RESULTS ANALYSIS

Simulation results are presented in this section to show the performance of the proposed control method applied to small scale vessels. Simulation experiments are carried out using Matlab 2018b. The model of the two tugs are represented by the "*TitoNeri*" developed by TU Delft [38], while the ship is represented by the "*CyberShip II*" [39]. The parameters of the vessel model and the towing system can be found in [26], the parameters of the control system are given in Table II, and the simulation settings are shown in Table III.

To highlight the importance of speed control for the towing process, we compare two scenarios, I and II. In scenario I, no speed profile is provided, the control objectives are the ship waypoint following, the ship heading adjusting and the towing system collision resolution. In scenario II, the proposed cooperative control scheme is used to manipulate the ship.

Fig. 3 shows the towing process of the two scenarios. In general, the trajectories in scenario II are smoother than those in scenario I, especially in the steering process (stage $W_{\text{p1}} \rightarrow W_{\text{p2}}$ and stage $W_{\text{p3}} \rightarrow W_{\text{p4}}$). In the first case of collision avoidance (detailed trajectories are shown in the top box), the static obstacle is successfully bypassed by the towing system in both scenarios. In the second case (detailed trajectories are shown in the bottom box), the towing system takes actions of starboard-side steering to avoid the dynamic obstacle in both scenarios, which complies with COLERGS rules. But we can infer from the trajectories that the towing system in scenario II has fewer fluctuations in the avoidance process. Comparing the time of arriving at each waypoint, scenario II has better efficiency than scenario I. Thus, although the two scenarios succeed to manipulate the ship to the desired states, scenario II (the proposed control scheme) shows better motion quality (smoother trajectories) and time efficiency.

The time-varying error of the ship position and the ship heading are shown in Fig. 4. In Fig. 4 (a), there are five curves for each scenario standing for the five times of waypoint following. At the end of each curve, the percentage error closes to zero, especially after the fifth blue dotted curve (the destination-point following task in Scenario II) reaches the red dashed line, its value is stable at zero. Fig. 4 (b) shows that the ship in both scenarios achieves the desired heading, but the oscillations in Scenario I are more than in Scenario II.

The time-varying linear velocities of the ship are shown in Fig. 5. The ship in Scenario II tracks the predefined surge profile from 0.15 m/s decreasing to 0.09 m/s and finally fixing at 0 m/s (Fig. 5 (a)). It is noticed that in the second collision avoidance case when the surge speed profile is updated (decreased from 0.09 m/s to 0.06 m/s), the ship still successfully tracks the new desired speed (around 530-620s). However, in Scenario I, the ship surge velocity shows five jagged shape changes. These "jags" come from the decreasing of the position errors in each waypoint following, which motivates the surge speed to vary from the highest to the lowest. When the towing system performs the steering operations, the ship sway velocity adjusts to high values in both scenarios (Fig. 5 (b)), but the oscillation in Scenario II is much smaller than Scenario I. Thus, there are frequent fluctuations of the trajectories for scenario I in Fig. 3 (a).

Fig. 6 shows the time-varying distance from the towing point of the two tugs to the towing point of the ship. The magnitude of the distance in Scenario I has large fluctuations at each waypoint changing, while in Scenario II, the distance

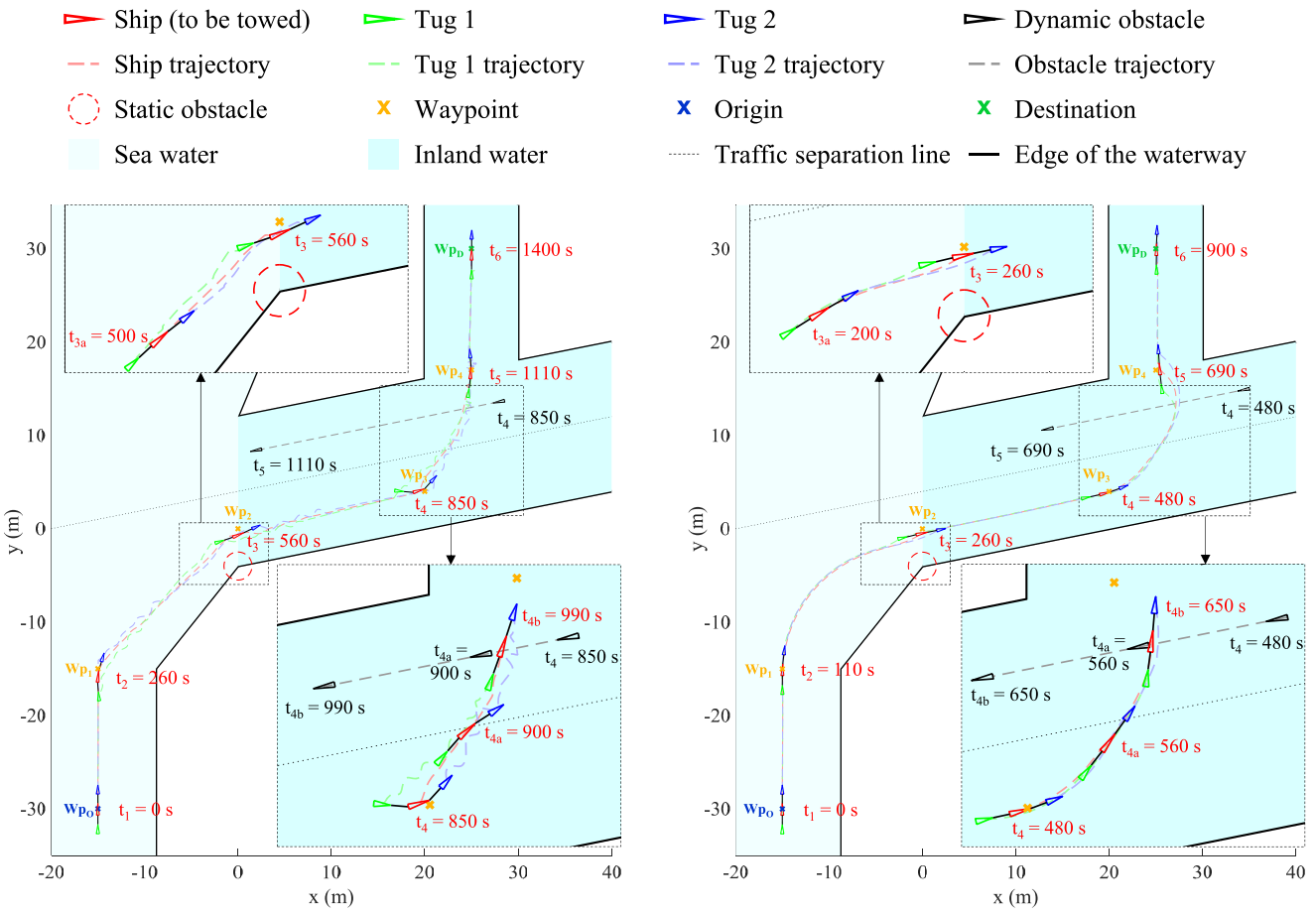

(a) Scenario I (b) Scenario II

Fig. 3. Towing process.

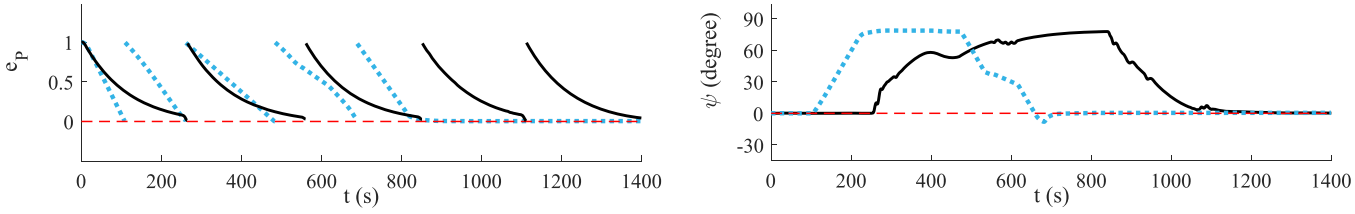

(a) Error of the ship position (b) Time-varying ship heading

Fig. 4. Performance of the ship waypoint following (a) and the ship heading adjusting (b), the red dashed line is the desired value, the black solid curve stands for Scenario I, the blue dotted curve stands for Scenario II.

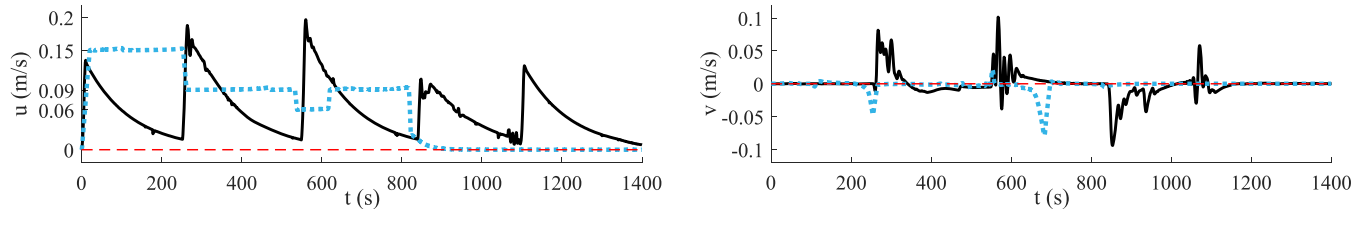

(a) Ship surge velocity (b) Ship sway velocity

Fig. 5. Time-varying linear velocities of the ship (the red dashed line is the final desired value, the black solid curve stands for Scenario I, the blue dotted curve stands for Scenario II).

change is always within a small range around the desired towline elongation (1 m).

Fig. 7 shows the normalized distance from the vessels in the towing system to the obstacles. From the static obstacle

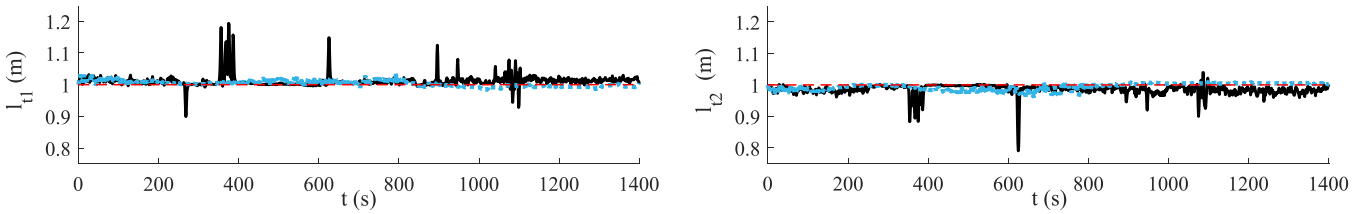

(a) Distance from the towing point of the tug 1 to the ship

(b) Distance from the towing point of the tug 2 to the ship

Fig. 6. Time-varying distance from the towing point of the tug to the towing point of the ship (the red dashed line is the desired value, the black solid curve stands for Scenario I, the blue dotted curve stands for Scenario II).

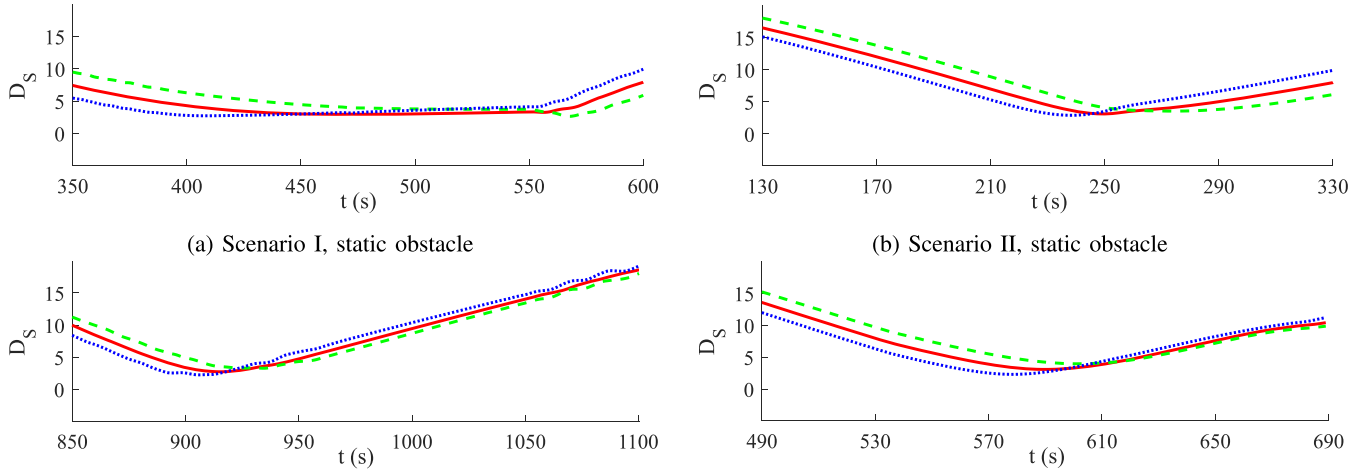

(a) Scenario I, static obstacle

(b) Scenario II, static obstacle

(c) Scenario I, dynamic obstacle

(d) Scenario II, dynamic obstacle

Fig. 7. Normalized distance from the vessels to the obstacles (the red solid line is the ship, the green dashed line is the tug 1, the blue dotted line is the tug 2).

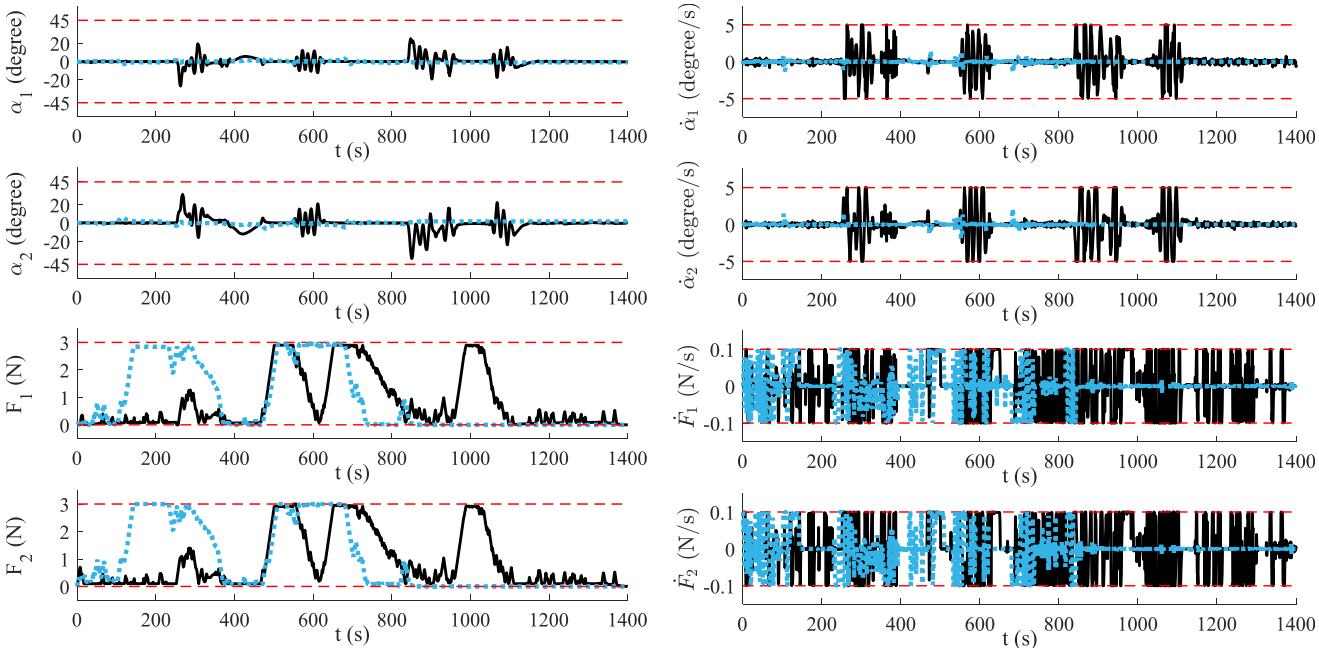

(a) Towing angles and forces

(b) Change rate of the towing angles and forces

Fig. 8. Control inputs of the ship (the red dashed line is the boundary given in the constraints, the black solid line stands for Scenario I, the blue dotted line stands for Scenario II): (a) Towing angles and forces; (b) Change rate of the towing angles and forces.

distance (Fig. 7 (a) and (b)), the duration of the close distance between the three vessels and the obstacle in Scenario I is longer; from the dynamic obstacle distance (Fig. 7 (c) and (d)), the minimum distance from the ship and tug 1 to the obstacle

TABLE IV
CONTROL PERFORMANCE WITH FIVE KPIS

Simulation Group	Waypoint Following	Heading Adjusting	Speed Profile Tracking	Consensus Reaching	Collision Resolution	
					Static Obstacle	Dynamic Obstacle
Scenario I	$e_{P1} = 1.15\%$ $e_{P2} = 3.04\%$ $e_{P3} = 2.69\%$ $e_{P4} = 0.64\%$ $e_{P5} = 0.79\%$	$e_\psi = 0.22°$	—	$e_{l1} = 19.35\%$ $e_{l2} = 20.93\%$	$D_S = 2.36$ $D_1 = 2.64$ $D_2 = 2.72$	$D_S = 2.73$ $D_1 = 4.11$ $D_2 = 2.82$
Scenario II	$e_{P1} = 0.41\%$ $e_{P2} = 2.09\%$ $e_{P3} = 0.31\%$ $e_{P4} = 3.18\%$ $e_{P5} = 0.57\%$	$e_\psi = 0.39°$	$e_u = 0.015$	$e_{l1} = 3.55\%$ $e_{l2} = 4.19\%$	$D_S = 2.48$ $D_1 = 3.55$ $D_2 = 2.90$	$D_S = 3.10$ $D_1 = 4.97$ $D_2 = 2.89$

is larger than Scenario II. The time varying control inputs of the ship and their change rates are shown in Fig. 8. It can be seen that the values of these variables are within the boundary in both scenarios, which satisfies the actuator saturation constraints defined in (18) – (21).

The control performances quantified by the KPIs defined in subsection III-E are shown in Table IV, we can infer that:

1) Each distance error in Scenario II is smaller than I, except the e_{P4}. The reason may come from the larger steering areas of avoiding the dynamic obstacle, meaning that the towing system in Scenario II obtains safer avoidance operations coming with the cost of space.
2) The heading error in both scenarios is quite small, so they have good performance in ship heading adjusting.
3) The RMSE of the surge speed in Scenario II is small, indicating the objective of the ship speed profile tracking is well achieved.
4) The error of the towline elongation in Scenario II is one-fifth of that in Scenario I, so the performance of consensus reaching in Scenario II is much better.
5) The minimum normalized distances from the three vessels to the obstacles in Scenario II are larger than in Scenario I, indicating that the towing process in Scenario II is safer.

Therefore, from the above results, the proposed control scheme succeeds multiple control objectives and shows better motion quality and time efficiency.

V. CONCLUSION AND FUTURE RESEARCH

This work focuses on multi-objective cooperative control of a multi-vessel ship-towing system. An ADMM-based multi-layer MPC approach with speed regulation is proposed to coordinate autonomous tugboats for manipulating a large ship to follow the waypoints, adjust the heading, track the speed profile, and resolve collisions in congested water traffic environments.

Such a complex multi-objective control problem is solved by the design of different controllers distributed in two layers. In the higher layer, the supervisory controller calculates the predicted towing forces and angles for the ship objectives of waypoint following, speed profile tracking, and collision resolution. The tug controller in the lower layer computes the thruster forces and moment for the tug system for the tug objectives of trajectory, surge speed tracking and collision resolution. The consensus between the lower-level and higher-level control is achieved by using the ADMM method through the iterations to make the predicted tug position and heading output by the tug controller approach to the desired tug trajectory output by the supervisory controller as much as possible. Simulation experiments indicate that the proposed control scheme coordinates multiple autonomous tugboats to transport a floating object smoothly and effectively and succeeds in multiple control objectives, in the meantime, the avoidance operation complies with COLREGS rules.

Future research will focus on the optimization of the proposed method: First, to consider the effect of environmental disturbances on the towing system to improve the robustness; Second, to formally analyze the feasibility of the proposed method (including environmental disturbances); Third, to validate its performance by applying it through actual model test experiment.

REFERENCES

[1] L. Chen, Y. Huang, H. Zheng, H. Hopman, and R. Negenborn, "Cooperative multi-vessel systems in urban waterway networks," *IEEE Trans. Intell. Transp. Syst.*, vol. 21, no. 8, pp. 3294–3307, Aug. 2020.
[2] M. Schiaretti, L. Chen, and R. R. Negenborn, "Survey on autonomous surface vessels: Part II—Categorization of 60 prototypes and future applications," in *Proc. Int. Conf. Comput. Logistics (ICCL)*, Southampton, U.K., 2017, pp. 234–252.
[3] Z. Du, V. Reppa, and R. R. Negenborn, "Cooperative control of autonomous tugs for ship towing," *IFAC-PapersOnLine*, vol. 53, no. 2, pp. 14470–14475, 2020.
[4] C. Lv *et al.*, "A hybrid coordination controller for speed and heading control of underactuated unmanned surface vehicles system," *Ocean Eng.*, vol. 176, pp. 222–230, Mar. 2019.
[5] M. E. N. Sorensen, M. Breivik, and B.-O.-H. Eriksen, "A ship heading and speed control concept inherently satisfying actuator constraints," in *Proc. IEEE Conf. Control Technol. Appl. (CCTA)*, Maui, HI, USA, Aug. 2017, pp. 323–330.
[6] W. B. Klinger, I. R. Bertaska, K. D. von Ellenrieder, and M. R. Dhanak, "Control of an unmanned surface vehicle with uncertain displacement and drag," *IEEE J. Ocean. Eng.*, vol. 42, no. 2, pp. 458–476, Apr. 2017.
[7] C. Lv, H. Yu, Z. Hua, L. Li, and J. Chi, "Speed and heading control of an unmanned surface vehicle based on state error PCH principle," *Math. Problems Eng.*, vol. 2018, pp. 1–9, Jan. 2018.
[8] S. Kragelund, V. Dobrokhodov, A. Monarrez, M. Hurban, and C. Khol, "Adaptive speed control for autonomous surface vessels," in *Proc. OCEANS-San Diego*, San Diego, CA, USA, 2013, pp. 1–10.
[9] Z. Peng, C. Meng, L. Liu, D. Wang, and T. Li, "PWM-driven model predictive speed control for an unmanned surface vehicle with unknown propeller dynamics based on parameter identification and neural prediction," *Neurocomputing*, vol. 432, pp. 1–9, Apr. 2021.

[10] T. S. Tiang and M. N. Mahyuddin, "Cooperative formation control algorithm of a generic multi-agent system applicable for multi-autonomous surface vehicles," in *Proc. IEEE Int. Conf. Underwater Syst. Technol., Theory Appl. (USYS)*, Penang, Malaysia, Dec. 2016, pp. 133–138.

[11] Y.-Y. Chen and Y.-P. Tian, "Formation tracking and attitude synchronization control of underactuated ships along closed orbits," *Int. J. Robust Nonlinear Control*, vol. 25, no. 16, pp. 3023–3044, 2015.

[12] K. Shojaei, "Leader–follower formation control of underactuated autonomous marine surface vehicles with limited torque," *Ocean Eng.*, vol. 105, pp. 196–205, Sep. 2015.

[13] X. Sun, G. Wang, Y. Fan, D. Mu, and B. Qiu, "A formation autonomous navigation system for unmanned surface vehicles with distributed control strategy," *IEEE Trans. Intell. Transp. Syst.*, vol. 22, no. 5, pp. 2834–2845, May 2021.

[14] Z. Qin, Z. Lin, D. M. Yang, and P. Li, "A task-based hierarchical control strategy for autonomous motion of an unmanned surface vehicle swarm," *Appl. Ocean Res.*, vol. 65, pp. 251–261, Apr. 2017.

[15] L. Chen, J. J. Hopman, and R. R. Negenborn, "Distributed model predictive control for vessel train formations of cooperative multi-vessel systems," *Transp. Res. C, Emerg. Technol.*, vol. 92, pp. 101–118, Jul. 2018.

[16] F. Arrichiello, H. K. Heidarsson, S. Chiaverini, and G. S. Sukhatme, "Cooperative caging and transport using autonomous aquatic surface vehicles," *Intell. Service Robot.*, vol. 5, no. 1, pp. 73–87, Jan. 2012.

[17] D. Zhang, L. Wang, J. Yu, and M. Tan, "Coordinated transport by multiple biomimetic robotic fish in underwater environment," *IEEE Trans. Control Syst. Technol.*, vol. 15, no. 4, pp. 658–671, Jul. 2007.

[18] H. Hajieghrary, D. Kularatne, and M. A. Hsieh, "Differential geometric approach to trajectory planning: Cooperative transport by a team of autonomous marine vehicles," in *Proc. Annu. Amer. Control Conf. (ACC)*, Milwaukee, WI, USA, Jun. 2018, pp. 858–863.

[19] M. G. Feemster and J. M. Esposito, "Comprehensive framework for tracking control and thrust allocation for a highly overactuated autonomous surface vessel," *J. Field Robot.*, vol. 28, no. 1, pp. 80–100, 2011.

[20] B. Bidikli, E. Tatlicioglu, and E. Zergeroglu, "Robust dynamic positioning of surface vessels via multiple unidirectional tugboats," *Ocean Eng.*, vol. 113, pp. 237–245, Feb. 2016.

[21] L. Chen, H. Hopman, and R. R. Negenborn, "Distributed model predictive control for cooperative floating object transport with multi-vessel systems," *Ocean Eng.*, vol. 191, Nov. 2019, Art. no. 106515.

[22] *Tugs and Tows—A Practical Safety and Operational Guide*, Shipowners' Club, London, U.K., 2015.

[23] R. H. Hansen, "DNV towing recommendations," Det Norske Veritas, Bærum, Norway, Tech. Rep. 7, 2014.

[24] A. N. Cockcroft and J. N. F. Lameijer, *A Guide to the Collision Avoidance Rules*. Oxford, U.K.: Elsevier, 2003.

[25] R. R. Negenborn and J. M. Maestre, "On 35 approaches for distributed MPC made easy," in *Distributed Model Predictive Control Made Easy* (Intelligent Systems, Control and Automation: Science and Engineering). Amsterdam, The Netherlands: Springer, 2013, pp. 1–37.

[26] Z. Du, R. R. Negenborn, and V. Reppa, "Cooperative multi-agent control for autonomous ship towing under environmental disturbances," *IEEE/CAA J. Autom. Sinica*, vol. 8, no. 8, pp. 1365–1379, Aug. 2021.

[27] Z. Du, V. Reppa, and R. R. Negenborn, "MPC-based COLREGS compliant collision avoidance for a multi-vessel ship-towing system," in *Proc. Eur. Control Conf. (ECC)*, Rotterdam, The Netherlands, Jun. 2021, pp. 1857–1862.

[28] Z. Du, R. R. Negenborn, and V. Reppa, "COLREGS-compliant collision avoidance for physically coupled multi-vessel systems with distributed MPC," *Ocean Eng.*, vol. 260, 2022, Art. no. 111917.

[29] Z. Du, R. R. Negenborn, and V. Reppa, "Multi-vessel cooperative speed regulation for ship manipulation in towing scenarios," in *Proc. 13th IFAC Conf. Control Appl. Mar. Syst., Robot., Vehicles (CAMS)*, Oldenburg, Germany, 2021, pp. 384–389.

[30] T. I. Fossen, *Handbook of Marine Craft Hydrodynamics and Motion Control*. Chichester, U.K.: Wiley, 2011.

[31] H. Hensen, *Tug Use in Port: A Practical Guide*. London, U.K.: Nautical Institute, 2003.

[32] S. Skjong and E. Pedersen, "Model-based control designs for offshore hydraulic winch systems," *Ocean Eng.*, vol. 121, pp. 224–238, Jul. 2016.

[33] A. Gambier, "Multiobjective optimal control of wind turbines: A survey on methods and recommendations for the implementation," *Energies*, vol. 15, no. 2, p. 567, Jan. 2022.

[34] Y. Liang, Z. Yin, and L. Nie, "Shared steering control for lane keeping and obstacle avoidance based on multi-objective MPC," *Sensors*, vol. 21, no. 14, p. 4671, Jul. 2021.

[35] X. Wang, J. Atkin, N. Bazmohammadi, S. Bozhko, and J. M. Guerrero, "Optimal load and energy management of aircraft microgrids using multi-objective model predictive control," *Sustainability*, vol. 13, no. 24, p. 13907, Dec. 2021.

[36] G. Yu, P. K. Wong, J. Zhao, X. Mei, C. Lin, and Z. Xie, "Design of an acceleration redistribution cooperative strategy for collision avoidance system based on dynamic weighted multi-objective model predictive controller," *IEEE Trans. Intell. Transp. Syst.*, vol. 23, no. 6, pp. 5006–5018, Jun. 2022.

[37] W. Ren, R. W. Beard, and E. M. Atkins, "A survey of consensus problems in multi-agent coordination," in *Proc. Amer. Control Conf.*, Portland, OR, USA, 2005, pp. 1859–1864.

[38] R. Skjetne, O. Smogeli, and T. I. Fossen, "Modeling, identification, and adaptive maneuvering of cybership II: A complete design with experiments," *IFAC Proc. Volumes*, vol. 37, no. 10, pp. 203–208, 2004.

[39] A. Haseltalab and R. R. Negenborn, "Model predictive maneuvering control and energy management for all-electric autonomous ships," *Appl. Energy*, vol. 251, Oct. 2019, Art. no. 113308.

Zhe Du received the B.Sc. degree in maritime administration and the M.Sc. degree in transport information engineering and control from the Wuhan University of Technology, Wuhan, China, in 2015 and 2018, respectively. He is currently pursuing the Ph.D. degree with the Department of Maritime and Transport Technology, Delft University of Technology, Delft, The Netherlands.

His research focuses on cooperative control of the physical-connected multi-vessel systems.

Rudy R. Negenborn received the M.Sc. degree in computer science/intelligent systems from Utrecht University in 1998 and the Ph.D. degree in distributed control for networked systems from the Delft University of Technology, Delft, The Netherlands, in 2007.

He is currently a Full Professor "multi-machine operations and logistics" with the Department of Maritime and Transport Technology, Delft University of Technology. His research interests are in the areas of distributed control, multi-controller systems, model predictive control, and optimization. He applies the developed theories to address control problems in large-scale transportation and logistic systems.

Vasso Reppa (Member, IEEE) received the Ph.D. degree in electrical and computer engineering from the University of Patras, Greece, in 2010. From 2011 to 2017, she was a Research Associate (now Research Affiliate) with the KIOS Research and Innovation Center of Excellence, Cyprus. In 2013, she was awarded the Marie Curie Intra European Fellowship and worked as a Research Fellow with CentraleSupélec, University of Paris-Saclay, France, from 2014 to 2016. She was a Visiting Researcher with Imperial College London, U.K., in 2015; and with The University of Newcastle, Australia, in 2016. She has been an Assistant Professor with the Department of Maritime and Transport Technology, Delft University of Technology, The Netherlands, since 2018. Her current research interests include multi-agent fault diagnosis and fault tolerant control, cooperative control, adaptive learning, observer-based estimation, and applications of autonomous systems in (waterborne) transport and smart buildings. She has been involved in several research and development projects (e.g., INTERREG "AVATAR," H2020 "NOVIMOVE," NWO "READINESS," and Marie Curie ITN "AUTOBarge").